Role of Bubble–Drop Interactions and Salt Addition in Flotation Performance

H. Chakibi, I. Hénaut, A. Salonen, D Langevin, J.-F. Argillier

▶ **To cite this version:**

H. Chakibi, I. Hénaut, A. Salonen, D Langevin, J.-F. Argillier. Role of Bubble–Drop Interactions and Salt Addition in Flotation Performance. Energy & Fuels, 2018, 32 (3), pp.4049-4056. 10.1021/acs.energyfuels.7b04053 . hal-04037125

HAL Id: hal-04037125
https://hal.science/hal-04037125

Submitted on 20 Mar 2023

HAL is a multi-disciplinary open access archive for the deposit and dissemination of scientific research documents, whether they are published or not. The documents may come from teaching and research institutions in France or abroad, or from public or private research centers.

L'archive ouverte pluridisciplinaire **HAL**, est destinée au dépôt et à la diffusion de documents scientifiques de niveau recherche, publiés ou non, émanant des établissements d'enseignement et de recherche français ou étrangers, des laboratoires publics ou privés.

Role of bubble-drop interactions and salt addition in flotation performance

H. Chakibi, I. Hénaut, A. Salonen*, D. Langevin*, J.-F. Argillier

Institut Français du Pétrole Energies Nouvelles, Av de Bois Préau, Rueil Malmaison, France

*Laboratoire de Physique des Solides, Université Paris Sud/Paris Saclay, Bâtiment 510, 91405 Orsay, France

Keywords : Flotation, bubble-drop adhesion, electrostatic interactions, salinity, pseudoemulsion film

Abstract

Gas flotation is an efficient technique used in the petroleum industry to remove oil contamination from produced water. This method is based on attaching air bubbles to oil droplets to make oil droplets rise faster. We investigated the role of water salinity in the efficiency of the process, using a model flotation column. We show that flotation efficiency increases with water salinity, highlighting the importance of the electrostatic repulsion between oil drops and air bubbles. We also studied the attachment between drops and bubbles, monitoring the temporal evolution of the thin films between them. Stable attachment requires that the water films formed between oil drops and air bubbles break and the oil spreads at the bubble surface. Increasing the salinity of the solution decreases the repulsion between the oil drops and the air bubbles, which in turn decreases the water film stability. The films rupture more readily, improving the drop-bubble attachment, and thus the flotation efficiency. The differences in water salinity can therefore lead to important changes in the flotation efficiency.

1. Introduction

Water and Oil & Gas production are strongly interdependent: water is both used and generated in this industry. On average, three to five water barrels are produced for each barrel of produced oil[1], which makes produced water the most important waste, in terms of volume. Water management is then one of the most challenging issues for oil companies. The two main options are either to treat the produced water in order to reinject it into the well or to discharge it overboard. Produced water composition is strongly dependent on the crude oil properties and water composition[2]. Produced water also contains many hazardous components such as dissolved hydrocarbons, emulsified crude oil, heavy metals, radioactive elements etc [3]. Therefore, the control of water treatment is not straightforward. The removal of oil contamination makes use of several gravitational processes. Stock tank separation eliminates the biggest oil droplets (diameters >150 µm). Hydrocyclones or centrifuges remove smaller droplets (20-150µm) and flotation the smallest ones (5-20µm). Gas flotation is very efficient as it allows to rapidly treat large quantities of produced waters. Induced and gas flotation are the most commonly used flotation technologies [4] [5]. Both methods are very effective in floating small suspended droplets [6]. An overview of oil water separation using gas flotation systems can be found in ref [7]. The methods are based on the collection of oil droplets by gas bubbles and their combined rise, which strongly accelerates oil creaming. In this case, gravitational separation is more difficult because the densities of oil and water are close. Furthermore, heavy oils contain surface active species able to stabilize very small drops. Flotation is more efficient when oil droplets spread at the bubble's surface, the attachment of drops is then more be robust and withstands better the upward rise [8]. According to Moosai and Dawe, the water film rupture is the rate governing steps of flotation: the rupture time must be smaller than the time during which the droplet and the bubble are in contact. The flow rates of air and oil droplets have therefore to be adjusted in order that contact events are long enough [8].

The water film rupture is related to the stability of the water films formed between approaching droplets and bubbles. These films thin and reach thicknesses below 100 nm, after which they eventually rupture[8]. In previous studies, the role of oil nature and content in water, drop size distribution and oil density has been investigated, with bubble size distribution, interfacial tensions, and the addition of surfactant and/or solid particles[8-9]. The rupture of films at thicknesses below 1µm is also likely affected by molecular forces between oil drops and gas bubbles [10], as in air-water-air films [11]or oil-water-oil films [12]. These forces depend on pH, which was indeed found to correlate with the flotation efficiency[13]. It was also remarked that rupture of the film between an oil drop and a gas bubble was easier at high water salinity and the effect was attributed to the lowering of the zeta potential of the drops by the compression of the double layer [14]. Recently, it was observed that

no film rupture is observed in ultrapure water, an effect attributed to electrostatic repulsion, which is assumed to be stronger in pure water due to hydroxyl ions adsorbed at the film surfaces [15]. So far, no detailed study of the role of salinity in flotation efficiency has been performed.

In this work, the role of molecular forces on the flotation process was investigated. In the film thickness range when rupture occurs, electrostatic forces are dominant. We have studied the role of these electrostatic forces by varying the salinity of water. We performed both macroscopic studies using a model flotation column and microscopic studies of the adhesion between bubbles and oil droplets. Consistent results were obtained with both approaches.

2. Theoretical background

The thin aqueous asymmetric films through which oil droplet and gas bubble interfaces interact are usually called pseudoemulsion films. Ross proposed two thermodynamic coefficients to predict the behavior of these films, the entering *E* and spreading *S* coefficients, defined as [16]:

$$E = \gamma_{w/a} + \gamma_{w/o} - \gamma_{o/a}$$
$$S = \gamma_{w/a} - (\gamma_{w/o} + \gamma_{o/a}) \quad (1)$$

where $\gamma_{w/a}$ is the surface tension between air and water, $\gamma_{w/o}$ is the interfacial tension between water and oil and $\gamma_{o/a}$ is the surface tension between oil and air. If *E* is positive, the oil droplet can enter the air/water surface, while if *S* is positive, the oil spreads on the bubble surface. These two coefficients are generally positive for crude oil/water/air films [14], favoring film rupture .

Lobo and Wasan [17] and Denkov[18] pointed out that the coefficient E only indicates if the energy is lowered after the drop enters the air-water interface: E has to be positive for the film to rupture, but it is not sufficient to determine whether they do or not. Indeed, *E* does not take into account the dynamics of film thinning and the interactions between film surfaces. When an oil droplet and a bubble approach, their interfaces are deformed and the pressure in the film differs from the surrounding pressure by a quantity equal to the capillary pressure [19]. The capillary pressure causes film thinning and when the film thickness falls below about 100nm, the forces between film surfaces become significant. At these distances, the force per unit surface is the sum of attractive van der Waals forces Π_{VDW} and electrostatic forces Π_{el} [20]:

$$\Pi(h) = \Pi_{VDW}(h) + \Pi_{el}(h) \quad (2)$$

This pressure is usually called disjoining pressure. The van der Waals contribution can be written as :

$$\Pi_{VDW}(h) = -\frac{H}{6\pi h^3} \quad (3)$$

H being an Hamaker constant. In the case of flotation, the two approaching particles are not identical and the electrostatic contribution to the disjoining pressure can be expressed by [20]:

$$\Pi_{el}(h) \sim 64\, n\, k_b T\, tanh\left(\frac{ze\Psi_o}{4k_bT}\right) tanh\left(\frac{ze\Psi_a}{4k_bT}\right) e^{-\kappa h} \quad (4)$$

with *n* the ion concentration, *z* their valency, k_b the Boltzmann's constant, *T* the absolute temperature, e the electron charge Ψ_o the potential of the oil- water interface, Ψ_a the potential of the air-water interface, *h* the film thickness, κ^{-1} the Debye length. As for two identical particles, this approximation is valid when the two ion concentration profiles differ only slightly from the case of single surfaces [21].

In practice, the measurement of the surface potentials Ψ_o and Ψ_a is not possible, and it is rather the zeta potentials ζ_o and ζ_a that are measured, using electrokinetic techniques, for instance studying the drop motion under an applied electric field [21] . In these measurements, one determines the potential at a certain distance from the surface since part of the counterions are entrained with the particle. Experience has shown that colloidal stability is however well correlated with this experimentally accessible potential[21].

Bubbles generated in aqueous solutions are negatively charged, with an iso-electric point about pH 4 [10]. This surface charge results from the adsorption of ionic species such as HCO_3^- from dissolved CO_2 [22]. The zeta potentialζ_a decreases with water pH, and, at constant pH, decreases when salt content increases [23].

The zeta potential of oil droplets depends on the oil chemical composition, on water pH and salinity and on the presence of surfactants, if added during oil recovery and treatment. Many crude oils contain polar components, like asphaltenes or naphthenic acids. When in contact with water, these organic molecules may get ionized [24], the extent of this ionization being related to the pKa of the species and to the water pH and salinity. Once dissociated, some organic polar components adsorb at the oil- water interface, others are transferred in the water phase. The surface charge and the amount transferred depend on the dissociation of the species, itself depending on pH and water salinity. When surfactant is present, the interface composition and charge can be modified [25].

The disjoining pressure of equation 2 has a maximum at a distance *h** between film surfaces, typically of order 10 nm. When the capillary pressure is larger than $\Pi(h^*)$, film thinning can proceed until film rupture. With pure fluids, when no electrostatic repulsion is present, film rupture occurs as

soon as the film thickness reached values where attractive van der Waals forces become significant [26]. In the case of oil-water-oil films containing ionic surface-active species, electrostatic forces are present. Denkov et al showed that the critical capillary pressure above which film rupture occurs is close to $\Pi(h^*)$ although lower by a factor of about 2.5 [12]. It is possible that during film thinning, mechanical or thermal fluctuations decrease locally the surface coverage, the repulsion being then lowered and film rupture allowed[27]. It should be noted that at very small distances h, the disjoining pressure contains a strongly repulsive term, generally of steric origin [28], which in principle should prevent film rupture. As for the electrostatic barrier, this repulsion could be suppressed by fluctuations in surface coverage[11]. Equations 2-4 are approximations that do not take into account the variations of the Hamaker constant and surface potential with distance, due to retardation effects and charge regulation [28] [21]. Other complications include hydrophobic forces and non-steric effects of adsorbed layers [28] It should be also noted that the solubility of gas in water and then the Hamaker constant change with salinity [3]. A discussion focused on flotation problems can be found in ref [29].

3. Materials and Methods

3.1 Preparation of synthetic produced waters

Brines were prepared using purified water from a Milli-Q system and salts NaCl (Fisher Chemicals, UK) and $CaCl_2$ (EMD Millipore Corp., Germany) of analytical grade with a purity greater than 99.9 %. We calculated the ionic strength of the brine as half the sum of the product of the concentrations and valencies of the different ions in the brine[21]. We prepared typical produced water using a stock oil in water emulsion containing 70 % oil and 30 % water, in weight. This concentrated emulsion is obtained using a previously described procedure [30] which permits to control the oil droplet size. The crude oil characteristics are given in Table 1. The oil is first heated to 60°C to lower its viscosity and facilitate its introduction into the mixing system. The oil droplets are stabilized with a nonionic surfactant, Triton X-405 (Sigma-Aldrich). Dodecane (VWR, rectapur GPR) was used to compare with crude oil. The surfactant is first dissolved in brine containing 7.5 g/L (130 mM) NaCl and its concentration in the stock emulsion is 1.2 wt %. The oil is dispersed in the aqueous phase using an Ultra-Turrax homogenizer, in a thermostated water bath at 60°C. The addition of oil is made slowly with syringes, while the agitation is maintained at 13400 rpm during 1-2 minutes and then at 24000 rpm during five minutes. The average droplet diameter of this stock emulsion is measured with a laser granulometer Mastersizer 2000, Malvern, and is 3.2 µm with a span of 1.4. In these experiments, the stock emulsion was diluted by the original brine (130 mM NaCl). Dilutions with pure

water were also used and led to the same drop size. This size is therefore robust and is not affected by the type of brine used to dilute the stock emulsion.

In order to obtain the model produced waters, the stock emulsion is diluted afterwards by gentle mixing in the brines until an oil concentration of 200 ppm and a residual concentration of Triton X-405 of 2.4 ppm. A picture of a produced water is presented Figure 1a.

The zeta potential of the oil droplets in the different model waters is measured with the Zetasizer, NANO-ZS, Malvern Instruments. As the critical micellar concentration of Triton X-405 is 2400 ppm, the surfactant remaining at the surface of the oil drops will desorb with time. The desorption time t_{des} can be estimated to be of the order of 10 minutes in the absence of convection. For this estimation, we have used $t_{des} \sim (1/D)\,(\Gamma/C)^2$, where D is the surfactant diffusion coefficient in water ($D \sim 4\ 10^{-10}$ m^2/s), Γ and C the surfactant concentrations respectively at the surface ($\Gamma \sim 1$ mg/m^2) and in the bulk [31]. Desorption is faster if convection is present, which is the case during the flotation experiments where bubbling induces strong mixing. Determinations of the zeta potential were also made with diluted emulsions containing 100 and 300 ppm surfactant, for which the estimated desorption times are respectively half an hour and 3 minutes for diffusion only. The samples were shaken before use, hence the desorption times were shorter. The measured values of the zeta potential were the same (within experimental error), confirming that surfactant was desorbed when the measurements were performed (a few minutes or longer after sample preparation). In all the experiments, oil drops can therefore be considered to be free of the Triton surfactant.

Density at 15°C (kg/cm^3)	969.7
API°	14
Acidity TAN – mg KOH/g	2.04
Elements analysis (%m/m)	
C	86.6
H	11.5
N	0.52
O	0.49
S	0.43
SARA - T>344°C (%m/m)	
Saturates	26.9
Aromatics	32.4
Resins	27.9
Asphaltenes C7	8.3

Table 1: Characteristics of the crude oil

3.2 Laboratory scale flotation tests

The flotation tests are made in a cylindrical glass column with an internal diameter of 6.7 cm (Figure 1b). Three taps allow sampling the produced water in order to quantify the flotation efficiency, at the column bottom. For all of our tests, air is injected at the bottom through a sintered glass filter whose pore size is 17-40 µm. The air flow rate is maintained at 40 l/h during the 10 minutes of an experiment.

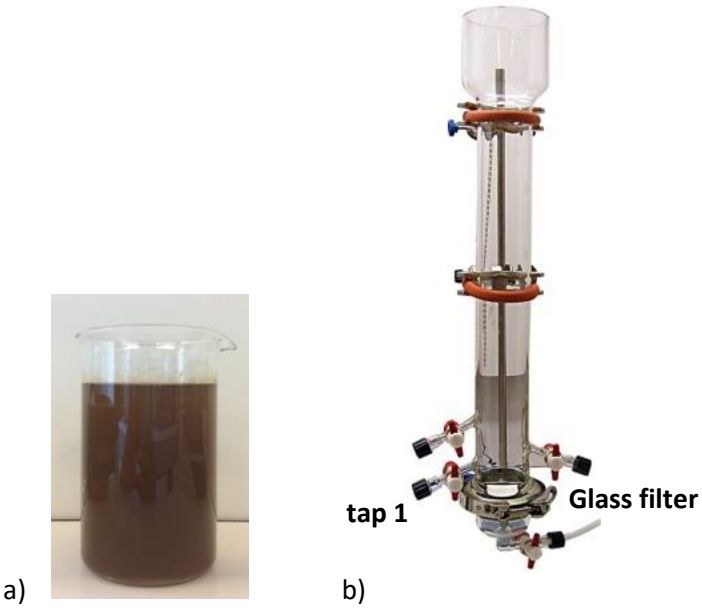

Figure 1: a) Prepared produced water containing 200 ppm crude oil; b) Laboratory scale flotation column with three taps and a glass filter, pore size: 17-40 µm

For each test, the model produced water is prepared just before the flotation. The water volume is fixed at 520 mL and the initial oil content is C_0 = 200 ppm. The produced water is introduced into the column from the top. Samples (about 10 mL) are taken every two minutes from the tap 1 of the column (Figure 1 b), the residual oil is extracted from water with dichloromethane and its concentration C_t at time t is determined by UV-visible absorbance with a spectrophotometer (DR 3800, Hach Lange). The process efficiency is quantified by plotting C_t/C_0 as a function of time.

3.3 Set up for the bubble-droplet adhesion

To study the adhesion of crude oil droplets and air bubbles during flotation, another set up was dedicated to the observation of oil droplets approaching an air-water interface. A millimetric oil droplet (diameter 6 mm +/- 0.4 mm) is formed with a syringe (needle diameter 0.9 mm) placed at the bottom of a glass cell filled with brine. We used about 50 drops, for which the spread in diameter values was ± 0.4 mm. The drop is left to rise freely under the influence of buoyancy from a constant distance (2 cm) to the air/water interface. This interface was made convex adding a hydrophobic

Teflon ring (diameter 35 mm) in order to prevent the lateral motion of the drop along the air-water interface.

To form a droplet with the syringe more easily, the crude oil has been diluted with xylene and the percentage of dilution has been varied between 10 and 20 wt %. The viscosities of the crude oil and of its dilutions were measured in a cone-plate rheometer (MCR 300, Anton Paar). These oils are all newtonian in the range of shear rates investigated (1-150 s^{-1}), their viscosities η_o are given in Table 2.

Xylene proportion (%)	Viscosity η_o (Pa.s)
0	15.5
10	1.14
15	0.48
18	0.35
20	0.25

Table 2 : Viscosity of the crude oil diluted by xylene

The different interfacial tensions were measured with crude oil containing 10% xylene and brines with 1, 3.4, 17 and 130 mM NaCl. In this way, the range of salinity of the flotation studies is covered. We used the pendent drop method with the tensiometer DSA 25, Krüss. As seen in Table 3, the tensions, the entry and spreading parameters do not depend significantly on the salinity of water. The coefficients *E* and *S* are positive over the whole salinity range, meaning that it is thermodynamically favorable for the oil to enter and spread on bubble surfaces.

[NaCl] (mM)	$\gamma_{w/a}$ (mN/m)	$\gamma_{o/a}$ (mN/m)	$\gamma_{o/w}$ (mN/m)	*E* (mN/m)	*S* (mN/m)
1.0	72	29	22	65	21
3.4	72	29	16	59	27
17.0	72	29	17	58	24
127.7	72	29	18	61	25

Table 3 : Measured surface tensions with brine and crude oil diluted with 10% xylene, with an accuracy of ± 2 mN/m. Calculated thermodynamic coefficients using equation 1 for [NaCl]=1 and 130mM.

Once it is in contact with the free surface, the pseudoemulsion film forms, gets thinner and eventually breaks. The different steps are shown in Figure 2. As in former studies[14-15], the time between the initial contact and film rupture is named rupture time τ.

Several techniques can be applied to evaluate τ, a survey can be found in [32]. In our setup, the evolution of the drop is recorded with a high-speed camera (300-400 frames per second). The radius of the oil covered area, r(t), is measured by analyzing the recorded movies. This study has been conducted for at least two oil drops for each ionic strength. The onsets of initial contact and film rupture can be determined within 2-3 frames, meaning that the rupture time can be determined with great accuracy (± 10 ms).

Oil droplet rise	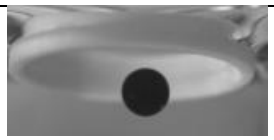
First collision, t=0 s	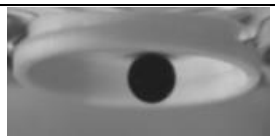
Film drainage	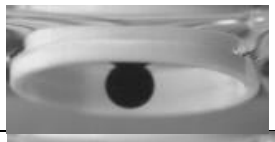
Film rupture t = τ	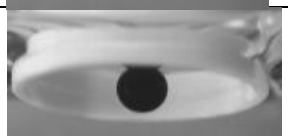
Oil spreading	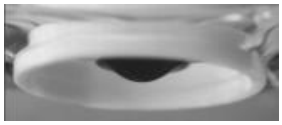

Figure 2 : Main steps for the attachment of an oil droplet at the surface air/water, [NaCl]= 1.0 mM

The droplet curvature is much higher than the curvature of the air/water surface and it can be considered that the air-water interface is planar, as in the flotation process, where the bubble curvature is much smaller than the oil droplet curvature. Other types of set up are used [14-15] where the oil droplets and/or bubbles are held by capillaries. The main drawback of these set ups is that drops are “manually” approached, so the initial film thickness may change between experiments. In our procedure the oil droplets have the same size and velocity (the water viscosity in not sensitive to the salt content, in this range of concentration) and the evolution of the pseudoemulsion film thickness is reproducible.

4. Results and discussion

4.1 Macroscopic scale

4.1.1 Flotation efficiency as a function of salinity

Model produced waters containing 200 ppm crude oil were prepared with different salt concentrations and injected into the flotation column. The resulting oil removal was characterized by the ratio C_t/C_0 and is plotted as a function of ionic strength in Figure 3. For a given time *t*, the residual oil concentration decreases when the ionic strength increases meaning that flotation efficiency increases with *I* up to 17 mM, after which it does not change significantly within error bars. Besides, for *I* higher than 17.0 mM, the final residual oil concentration after 10 minutes C_{10} is very low (C_{10}/C_0 < 0.05) and the produced water can be considered as clean.

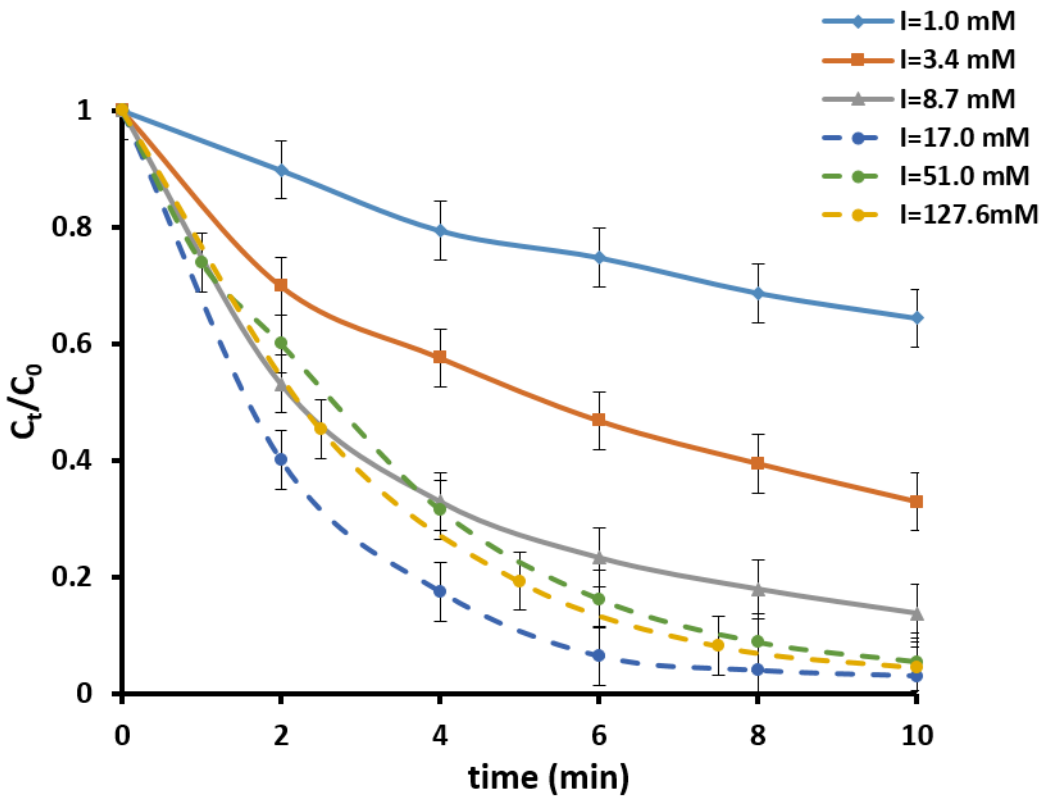

Figure 3: Normalised flotation efficiency Ct/C_0 in time in solutions with different concentrations I of NaCl

4.1.2 *Effect of bubble size*

Flotation is known to be more efficient with small and homogenously dispersed bubbles [6]. The flotation efficiency increase seen in Figure 3 could therefore be due to a change in bubble size. Indeed, at high salinity, the generated air bubbles were smaller than at low salinity. This is a well-known effect in salty water (no added oils): many common salts like NaCl or $CaCl_2$ inhibit bubble coalescence above C_s^* (a salt dependent transition concentration)[33] [34] [35]. If this concentration is defined as the value corresponding to 50% coalescence, C_s^*= 78 mM for NaCl and 38 mM for $CaCl_2$. The role of salt has been recently elucidated[36]. To investigate the influence of salinity on bubble size and dispersion in our flotation column, the previous experiments were repeated with water free from crude oil. In this case, the liquid is transparent and images of the bubbles can be taken and analyzed using a high speed camera (400 images/s). We obtain in this way an average bubble diameter d, which is plotted as a function of the ionic strength in Figure 4 for brines with NaCl.

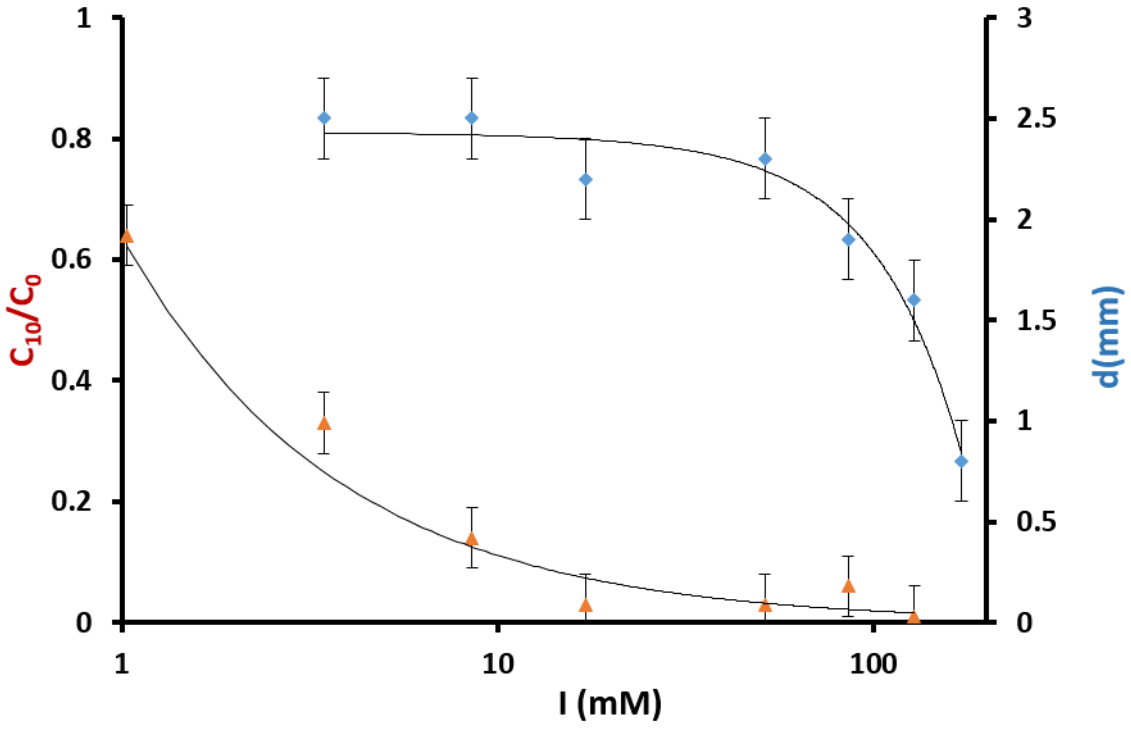

Figure 4 : Comparison between the evolutions of the average bubble diameter (*d*) and C_{10}/C_0 with NaCl concentration, C_{10} being the oil concentration after 10 minutes of flotation.

The bubble size remains constant until *I* = 50 mM above which it decreases due to coalescence inhibition in agreement with literature data. However, the change in bubble size does not occur in

the same salinity range as that of the flotation efficiency. Indeed, as it can be seen on Figure 4, the bubble size is constant between 3 and 50 mM while flotation efficiency increases significantly. This suggests that the inhibition of bubble coalescence by the salt does not play a role in the flotation experiments presented. The efficiency could of course be improved above 50 mM by the decrease in bubble size, but it is already very good well before, and no difference in efficiency can be evidenced above 17 mM within experimental error.

4.1.3 Zeta potential of oil droplets in produced water

As discussed in section 2 and in the introduction, the adhesion between oil drops and bubbles depends on the stability of the pseudoemulsion film that forms between them, which behavior is governed by the interactions between the film surfaces. It can therefore be expected that flotation is impacted by these interactions, and in particular by the zeta potential of oil droplets and air bubbles.

The crude oil droplet zeta potential has been measured for two different brines containing either monovalent (NaCl) or divalent ($CaCl_2$) salt (Figure 5).

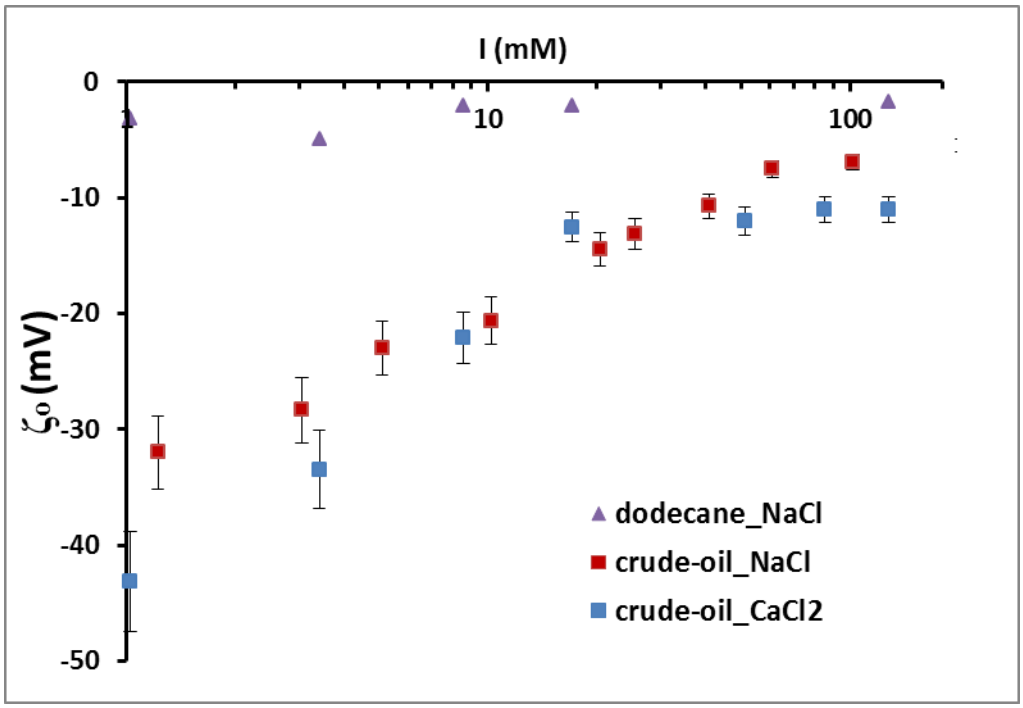

37

Figure 5 : Zeta potential of crude oil droplets in brines at different ionic strengths ; NaCl (red squares) and $CaCl_2$ (blue squares). Zeta potential of dodecane droplets in NaCl brine (violet triangles).

In each case, a negative value is obtained due to the ionization of polar species contained in the crude oil. The absolute value of the zeta potential decreases when the ionic strength increases. This trend is reinforced with divalent calcium ions possibly because one calcium ion is able to associate with two naphtenate or carboxylate ions [38]. When the oil does not contain any polar species, the zeta

potential of droplets is close to zero and does not change with salinity. This has been demonstrated by measuring the zeta potential of pure dodecane droplets within NaCl brines (Figure 5). Note that the values measured are smaller (in absolute value) than those reported by Marinova et al, that were attributed to the present of OH- ions at the interface[39]. In this earlier work, very pure oils were used, and it is likely that the residual surface active contaminants in the dodecane used in our work displaced the OH- ions as usually observed with very small amounts of added surfactant

In Figure 6, the evolution of C_{10}/C_0 is represented as a function of oil droplet zeta potential.

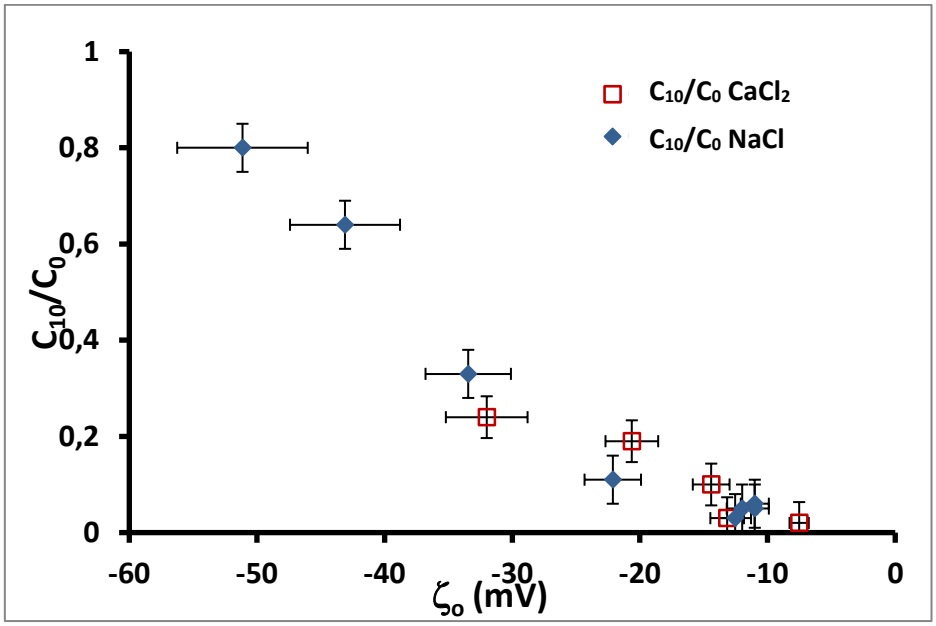

Figure 6: Evolution of the normalized flotation efficiency C_{10}/C_0 with the oil droplet zeta potential, in NaCl (blue lozenges) and CaCl2 (red squares) brines

We observed that, independently of the cation nature, there is a good correlation between oil droplet zeta potential and C_{10}/C_0: this ratio decreases with the absolute value of ζ_o. When the strength of electrostatic repulsions decreases, oil droplets and air bubbles attach more easily and rise faster leaving clear water at the bottom of the column.

4.2 Micrometric scale

4.2.1 Bubble-drop attachment process

To better understand the mechanism of the attachment between an oil droplet and an air bubble, the approach of oil drops toward an air-water interface has been studied. The rupture times have been measured with the protocol described in the Materials and Methods section. This protocol has

been applied to droplets of diluted crude oil in xylene with different concentrations (10, 15, 18 and 20 wt %) and brines containing different amounts of NaCl. The rupture time values are plotted as a function of ionic strength in Figure 7.

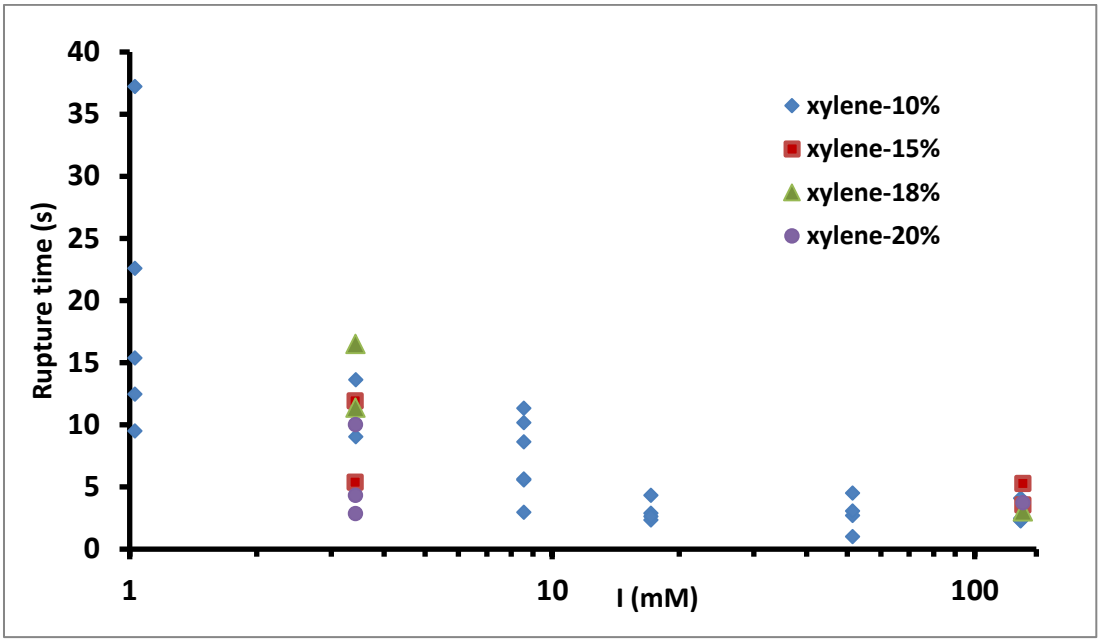

Figure 7: Oil film rupture times for droplets of diluted crude oil in xylene, at the interface between air and NaCl brines.

It can first be noticed that the dispersion of the measured rupture times is large. This is a general feature in the rupture of thin liquid films and is due to the fact that the rupture is produced either by random mechanical or thermal fluctuations [11].

Figure 7 shows that the rupture times do not appear to depend on the oil viscosity, but they appreciably decrease with ionic strength, becoming quite small above 17 mM. Interestingly, this ionic strength corresponds to the low zeta potentials and also the onset of best oil removal. These results suggest that the pseudoemulsion film rupture is mostly governed by interfacial electrostatics. There should also be an important short-range repulsion due to the surface-active species originating from the oil phase, but as in many other cases, this repulsion is unable to protect the film from rupture.

When considering the expression of the disjoining pressure (equations 2-4), one finds that there is a maximum of $\Pi(h)$ at a distance h^* between film surfaces, which strongly depends on the salinity. When the capillary pressure becomes larger than Π^*, the film should rupture. In order to evaluate Π^*, the value of the Hamaker constant is needed. This constant has been measured for bitumen emulsions and found quite high, about 10^{-19}J (20 k_bT) [40]. In order to obtain the oil-water-air Hamaker constant, combinations of different values are needed [21] and in view of all the uncertainties, we have just assumed that $H\sim$ 10 k_bT ~$4*10^{-20}$ J. The surface potentials Ψ_a and Ψ_o were assumed to be close

to the zeta potentials ζ_a and ζ_o. We have taken for ζ_a the value quoted in Graciaa et al. work [41] at the pH of our solutions (5.5), which does not vary appreciably with salinity, $\zeta_a \sim$- 25 mV. We used for ζ_o the values shown in Figure 5 and reported in Table 4. The values calculated for Π^* are reported in Table 4. More details about the calculations can be found in the supplementary information (SI).

I (mM)	ζ_o (mV)	Π^*(10^3 Pa)
1.0	-43	36
3.4	-33	54
8.7	-22	24
17.0	-13	_

Table 4. Zeta potentials and disjoining pressure barriers calculated using equations 2 and 3. See SI for more details

The value of Π^* is rather high at low salinity and decrease appreciably with salinity, vanishing around 17 mM. It must be stressed that the non-monotonous variation seen in table 4 should be considered with care, as the values of Π^* depend critically on the DLVO parameters, which are not known precisely. The values shown in the table however explain why the coalescence between oil drops and bubbles become easier at high salinity. The evolution of the zeta potential ζ_o is similar , justifying the good correlation between this potential and both flotation efficiency and pseudoemulsion film stability. This remarkable correlation may seem surprising since the capillary pressures encountered during the flotation of bubbles and in the pseudo emulsion films are different: the oil drops in the flotation experiment have diameters of the order of microns, while in the oil drop rise experiment, the diameters are millimetric. Clearly more work is needed to better understand the role of capillary pressure in both types of experiments. These results confirm however the interest of using the rupture time as a tool for evaluating flotation efficiency.

4.2.2 Oil spreading

After the pseudoemulsion film rupture, the oil spreads and covers the water/air surface, consistent with the fact that the spreading coefficient *S* is positive (Table 3). The time evolution of the ratio between the initial oil droplet radius R_d and the radius of the oil covered area *r(t)* is shown in Figure 8 for different NaCl concentrations and for xylene containing 10% crude oil. All the curves superimpose demonstrating that the oil spreading on the water/air interface speed is not sensitive to salinity. This is consistent with the quasi constant value of the coefficient *S* = 21-27 mN/m in the salinity range studied.

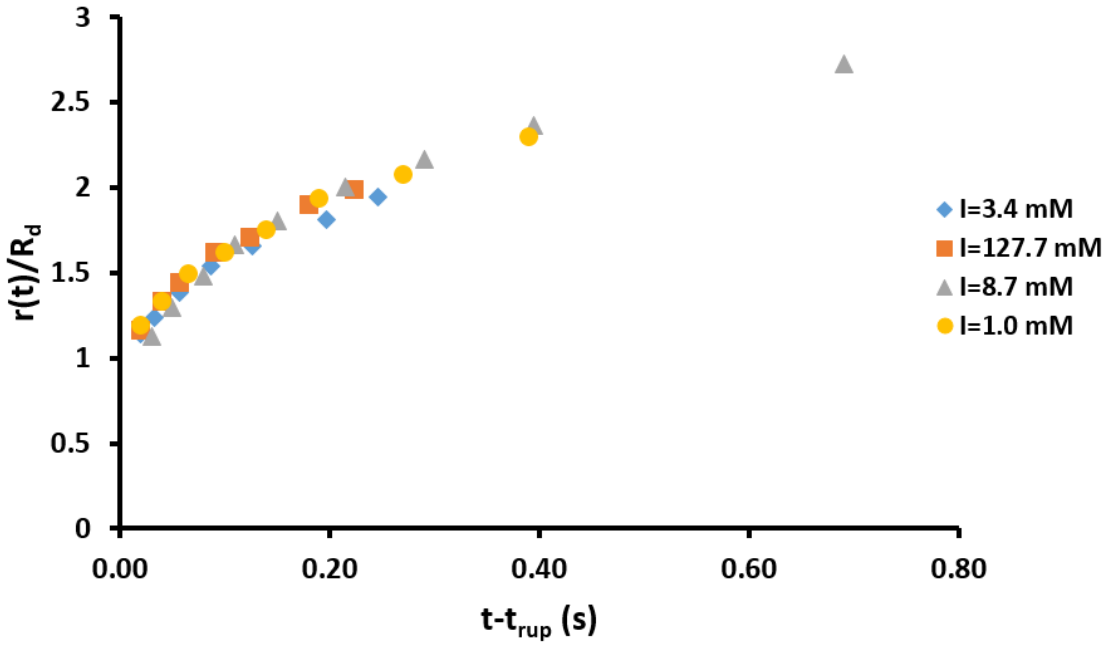

Figure 8 : Evolution of the radius of the oil drop at the air-water surface in solutions of different NaCl concentrations

To investigate the influence of oil viscosity on the oil spreading, experiments were repeated with the three other xylene diluted oils. In contrast to rupture times that remain constant upon oil dilution (Figure 7), spreading velocities decrease when the oil viscosity increases. These results are in agreement with the observations of Eftekhardadkhah and Oye [15] who reported that oil spreading proceeded with a velocity inversely proportional to the oil viscosity. Here, Figure 8 suggests that the radius r does not increase linearly with time. A complete analysis is presented in the supplementary information. The radius varies as $r(t)/R_d = (t/T)^{1/2}$ with $T = \eta_o R_d/(2\gamma_{ow})$, and the radius increases as the square root of the oil viscosity. Results of this analysis are given in Table 5.

Xylene proportion (%)	Viscosity (Pa.s)	Theoretical slope (s^{-1}) ($2\gamma_{ow}/\eta_o R$)	Experimental slope(s^{-1})
10	1.14	11.7	10.5
15	0.48	28	24
18	0.35	38	40
20	0.25	53	53

Table 5: Correlation between oil spreading speed and oil viscosity

One sees in Table 5 that the agreement between theory and experiment is remarkable.

Eftekhardadkhah and Oye observed however that the flotation efficiency did not depend significantly on the oil viscosity. This could be because the rupture times are longer than the spreading times. Indeed here, after 0.2 s, the oil has spread appreciably, and since the spreading radius is inversely proportional to the viscosity, one could estimate that the crude oil will have spread in 0.7 s, a time shorter than the rupture time at low salinity and comparable at high salinity.

5. Conclusion

We have studied the influence of the water salinity on the efficiency of flotation as a water purification method to remove small drops of crude oil. The results obtained with a macroscopic experiment of a flotation column and with individual oil droplets are in good agreement; increased salinity leads to improved attachment of the gas bubbles to the emulsion drops. An increase in salinity results in a decrease of the zeta potential of the oil droplet, so electrostatic repulsions between the oil droplet and the air bubble are weakened. The pseudoemulsion film rupture is easier, attachment improved and the flotation is more efficient.

The increase of flotation efficiency is not linked to a change in size of gas bubbles, because in the range of salt concentrations where the efficiency is most improved by the increase of salinity the bubble size is constant. The flotation efficiency is mostly governed by the pseudoemulsion film stability. There is a surprisingly good correlation of both rupture time of the singe films and the flotation efficiency in a column with the oil droplets zeta potential, despite the differences in capillary pressures between both types of measurements.

The time for oil spreading after film rupture is smaller or comparable to the film rupture time. This result confirms that the water film rupture is the main rate governing step in flotation, as postulated in former studies.

Acknowledgments

We thank IFPEN colleagues Jean Tricard, Nathalie Palazzo, Brigitte Betro and Sylvie Perrin for their help in the design of the experiments and many interesting discussions as well as Maxime Schneider from U. of Saclay.

References

1. Fakhru'l-Razi, A.; Pendashteh, A.; Abdullah, L. C.; Biak, D. R. A.; Madaeni, S. S.; Abidin, Z. Z., Review of technologies for oil and gas produced water treatment. *Journal of Hazardous Materials* **2009,** *170* (2), 530-551.
2. Dudek, M.; Kancir, E.; Oye, G., Influence of the Crude Oil and Water Compositions on the Quality of Synthetic Produced Water. *Energy & Fuels* **2017,** *31* (4), 3708-3716.
3. Hansen, B. R.; Davies, S. R. H., Review of potential technologies for the removal of dissolved components from produced water. *Chemical Engineering Research & Design* **1994,** *72* (A2), 176-188.
4. Rawlins, C. H., Flotation of fine oil droplets in petroleum production cir-cuits. *Recent Advances in Mineral Processing Plant Design,Society for Mining, Metallurgy, and Exploration* **2009**, 232-246.
5. Wang, L. K. S., N.K.; Selke,W.A.; Aulenbach,D.B.; , Flotation Technology. *HumanaPress* **2010**.
6. Strickland, W. T., Laboratory results of cleaning produced water by gas flotation. *Society of Petroleum Engineers Journal* **1980,** *20* (3), 175-190.
7. Saththasivam, J.; Loganathan, K.; Sarp, S., An overview of oil-water separation using gas flotation systems. *Chemosphere* **2016,** *144*, 671-680.
8. Moosai, R.; Dawe, R. A., Gas attachment of oil droplets for gas flotation for oily wastewater cleanup. *Separation and Purification Technology* **2003,** *33* (3), 303-314.
9. (a) Koczo, K.; Lobo, L. A.; Wasan, D. T., Effect of oil on foam stability - aqueous foams stabilized by emulsions. *Journal of Colloid and Interface Science* **1992,** *150* (2), 492-506; (b) Eftekhardadkhah, M.; Aanesen, S. V.; Rabe, K.; Oye, G., Oil Removal from Produced Water during Laboratory- and Pilot-Scale Gas Flotation: The Influence of Interfacial Adsorption and Induction Times. *Energy & Fuels* **2015,** *29* (11), 7734-7740.
10. Tabor, R. F.; Wu, C.; Lockie, H.; Manica, R.; Chan, D. Y. C.; Grieser, F.; Dagastine, R. R., Homo- and hetero-interactions between air bubbles and oil droplets measured by atomic force microscopy. *Soft Matter* **2011,** *7* (19), 8977-8983.
11. Langevin, D., Bubble coalescence in pure liquids and in surfactant solutions. *Current Opinion in Colloid & Interface Science* **2015,** *20* (2), 92-97.
12. Tcholakova, S.; Denkov, N. D.; Ivanov, I. B.; Campbell, B., Coalescence stability of emulsions containing globular milk proteins. *Advances in Colloid and Interface Science* **2006,** *123*, 259-293.
13. Zouboulis, A. I.; Avranas, A., Treatment of oil-in-water emulsions by coagulation and dissolved-air flotation. *Colloids and Surfaces a-Physicochemical and Engineering Aspects* **2000,** *172* (1-3), 153-161.
14. Oliveira, R. C. G.; Gonzalez, G.; Oliveira, J. F., Interfacial studies on dissolved gas flotation of oil droplets for water purification. *Colloids and Surfaces a-Physicochemical and Engineering Aspects* **1999,** *154* (1-2), 127-135.
15. Eftekhardadkhah, M.; Oye, G., Induction and Coverage Times for Crude Oil Droplets Spreading on Air Bubbles. *Environmental Science & Technology* **2013,** *47* (24), 14154-14160.
16. Ross, S., Inhibition of foaming .2. a mechanism for the rupture of liquid films by antifoaming agents. *Journal of Physical and Colloid Chemistry* **1950,** *54* (3), 429-436.
17. Lobo, L.; Wasan, D. T., Mechanisms of aqueous foam stability in the presence of emulsified non-aqueous-phase liquids - structure and stability of the pseudoemulsion film. *Langmuir* **1993,** *9* (7), 1668-1677.
18. Denkov, N. D., Mechanisms of foam destruction by oil-based antifoams. *Langmuir* **2004,** *20* (22), 9463-9505.
19. Chan, D. Y. C.; Klaseboer, E.; Manica, R., Film drainage and coalescence between deformable drops and bubbles. *Soft Matter* **2011,** *7* (6), 2235-2264.
20. Verwey, E. J. W.; Overbeek, J. T. G., *Theory of the stability of lyophobic colloids*. Elsevier: Amsterdam, 1948.
21. Evans, F.; Wennerström, W., *The Colloidal Domain*. second ed.; Wiley: 1999.

22. Katsir, Y.; Marmur, A., Rate of Bubble Coalescence following Quasi-Static Approach: Screening and Neutralization of the Electric Double Layer. *Scientific Reports* **2014,** *4*.
23. Yang, C.; Dabros, T.; Li, D. Q.; Czarnecki, J.; Masliyah, J. H., Measurement of the zeta potential of gas bubbles in aqueous solutions by microelectrophoresis method. *Journal of Colloid and Interface Science* **2001,** *243* (1), 128-135.
24. Hutin, A.; Argillier, J.-F.; Langevin, D., Mass Transfer between Crude Oil and Water. Part 1: Effect of Oil Components. *Energy & Fuels* **2014,** *28* (12), 7331-7336.
25. Hutin, A.; Argillier, J.-F.; Langevin, D., Mass Transfer between Crude Oil and Water. Part 2: Effect of Sodium Dodecyl Benzenesulfonate for Enhanced Oil Recovery. *Energy & Fuels* **2014,** *28* (12), 7337-7342.
26. Vakarelski, I. U.; Manica, R.; Tang, X. S.; O'Shea, S. J.; Stevens, G. W.; Grieser, F.; Dagastine, R. R.; Chan, D. Y. C., Dynamic interactions between microbubbles in water. *Proceedings of the National Academy of Sciences of the United States of America* **2010,** *107* (25), 11177-11182.
27. Bergeron, V., Forces and structure in thin liquid soap films. *Journal of Physics-Condensed Matter* **1999,** *11* (19), R215-R238.
28. Israelachvili, J., *Intermolecular and Surface Forces* second ed.; Academic Press: 1992.
29. Nguyen, A. V.; Schulze, H. J., *Colloidal science of flotation*. Marcel Dekker: New York, 2004.
30. Boufarguine, M.; Noïk, C.; Dalmazzone, C.; Argillier, J.-F. o.; Mouazen, M.; Hénaut, I., *Methodological Approach for Analyzing the Impact of Chemical EOR on Surface Processes*. 2013; Vol. 2.
31. He, Y.; Yazhgur, P.; Salonen, A.; Langevin, D., Adsorption-desorption kinetics of surfactants at liquid surfaces. *Advances in Colloid and Interface Science* **2015,** *222*, 377-384.
32. Verrelli, D. I.; Albijanic, B., A comparison of methods for measuring the induction time for bubble-particle attachment. *Minerals Engineering* **2015,** *80*, 8-13.
33. Craig, V. S. J.; Ninham, B. W.; Pashley, R. M., The effect of electrolytes on bubble coalescence in water. *Journal of Physical Chemistry* **1993,** *97* (39), 10192-10197.
34. Craig, V. S. J.; Henry, C. L., Specific Ion Effects at the Air–Water Interface: Experimental Studies. In *Specific Ion Effects*, WORLD SCIENTIFIC: 2011; pp 191-214.
35. Henry, C. L.; Craig, V. S. J., The Link between Ion Specific Bubble Coalescence and Hofmeister Effects Is the Partitioning of Ions within the Interface. *Langmuir* **2010,** *26* (9), 6478-6483.
36. Katsir, Y.; Marmur, A., Rate of Bubble Coalescence Following Dynamic Approach: Collectivity-Induced Specificity of Ionic Effect. *Langmuir* **2014,** *30* (46), 13823-13830.
37. Stubenrauch, C.; Rojas, O. J.; Schlarmann, J.; Claesson, P. M., Interactions between nonpolar surfaces coated with the nonionic surfactant hexaoxyethylene dodecyl Ether C12E6 and the origin of surface charges at the air/water interface. *Langmuir* **2004,** *20* (12), 4977-4988.
38. Jafvert, C. T.; Westall, J. C.; Grieder, E.; Schwarzenbach, R. P., Distribution of hydrophobic ionogenic organic-compounds between octanol and water - organic-acids. *Environmental Science & Technology* **1990,** *24* (12), 1795-1803.
39. Marinova, K. G.; Alargova, R. G.; Denkov, N. D.; Velev, O. D.; Petsev, D. N.; Ivanov, I. B.; Borwankar, R. P., Charging of oil-water interfaces due to spontaneous adsorption of hydroxyl ions. *Langmuir* **1996,** *12* (8), 2045-2051.
40. Salou, M.; Siffert, B.; Jada, A., Study of the stability of bitumen emulsions by application of DLVO theory. *Colloids and Surfaces a-Physicochemical and Engineering Aspects* **1998,** *142* (1), 9-16.
41. Graciaa, A.; Morel, G.; Saulner, P.; Lachaise, J.; Schechter, R. S., The zeta-potential of gas-bubbles. *Journal of Colloid and Interface Science* **1995,** *172* (1), 131-136.